

# Healable Cellulose Iontronic Hydrogel Stickers for Sustainable Electronics on Paper

*Inês Cunha, Jorge Martins, Diana Gaspar, Pydi Ganga Bahubalindrani, Elvira Fortunato, Rodrigo Martins, and Luís Pereira\**

**Novel nature-based engineered functional materials combined with sustainable and economically efficient processes are among the great challenges for the future of mankind. In this context, this work presents a new generation of versatile flexible and highly conformable regenerated cellulose hydrogel electrolytes with high ionic conductivity and self-healing ability, capable of being (re)used in electrical and electrochemical devices. They can be provided in the form of stickers and easily applied as gate dielectric onto flexible indium–gallium–zinc oxide transistors, decreasing the manufacturing complexity. Flexible and low-voltage (<2.5 V) circuits can be handwritten on-demand on paper transistors for patterning of conductive/resistive lines. This user-friendly and simplified manufacturing approach holds potential for fast production of low-cost, portable, disposable/recyclable, and low-power ion-controlled electronics on paper, making it attractive for application in sensors and concepts such as the “Internet-on-Things.”**

some of the electronic systems in the future, envisioning a balance between well-being, environment, economy, and societal acceptance.<sup>[1]</sup>

Countless efforts have been made to develop a sustainable generation of less complex, low-power, autonomous, wireless, flexible, and affordable multifunctional smart systems. These key features are of major importance in the emerging field of the “Internet-of-Things” (IoTs), the networking of smart objects, as a tool to bring comfort and welfare to citizens.<sup>[2–4]</sup> It is of great importance such smart systems to be reusable, recyclable, disposable (biodegradable), and made from abundant, highly stable, and neither harmful nor polluting materials, such as polysaccharides.<sup>[3–6]</sup>

Among the various polysaccharides, cellulose stands out as the most abundant biopolymer resource on Earth, commonly used in the form of paper, which is increasingly considered as a suitable starting building block for the design of eco-friendly and sustainable advanced functional materials.<sup>[6–9]</sup> The abundant charged hydrophilic functional groups, including hydroxyl, carboxyl, and aldehyde groups, in the polymer chain of cellulose and its derivatives can be used to prepare hydrogels.<sup>[9,10]</sup> Hydrogel materials are crosslinked 3D hydrophilic polymeric networks capable of absorbing large amounts of water (or biological fluids) and swelling in a reversible manner. These materials have both wet and soft appearance and can exhibit fascinating properties, such as high-water absorption capacity, stretchability, moldability, stimuli-responsiveness, and self-healing.

Hydrogels with healing functionality are of foremost interest to the next generation electronic devices as they can repair themselves in response to an external stimulus (e.g., light, heat, solvent, pH, or pressure), and regain mechanical and functional properties upon local damage.<sup>[10–16]</sup> Thus, they can lead to waste reduction by extending the lifetime of products, while avoiding failure of materials during use and even safety problems. This property can be achieved by introducing reversible chemical bonds, such as hydrogen and ionic bonding, supramolecular interactions, molecular diffusion, and/or chain entanglement.<sup>[12]</sup> Self-healable hydrogels can be integrated into functional electronic devices,<sup>[10–25]</sup> from sensors, artificial electronic skins, soft robotics, solar cells, actuators, and energy devices to transistors.

In particular, ionic hydrogels have been considered a promising class of gate dielectrics able to drastically reduce the

## 1. Introduction


Modern society lives engulfed in a world strongly dependent on electronics, where consumerism allied with an inappropriate management at the end of life of products is causing a great stress in the planet resources. Thus, there is an urgency to find sustainable solutions that can be implemented in

I. Cunha, J. Martins, Prof. E. Fortunato, Prof. R. Martins, Prof. L. Pereira  
CENIMAT/i3N

Departamento de Ciência dos Materiais  
Faculdade de Ciências e Tecnologia, FCT  
Universidade Nova de Lisboa and CEMOP-UNINOVA  
Campus da Caparica, Caparica 2829-516, Portugal  
E-mail: [lmnp@fct.unl.pt](mailto:lmnp@fct.unl.pt)

Dr. D. Gaspar, Prof. L. Pereira  
AlmaScience  
Campus da Caparica, Caparica 2829-516, Portugal

Prof. P. G. Bahubalindrani  
Indian Institute of Technology Goa  
Goa College of Engineering Campus  
Farmagudi, Ponda, Goa 403401, India

 The ORCID identification number(s) for the author(s) of this article can be found under <https://doi.org/10.1002/aelm.202001166>.

© 2021 The Authors. Advanced Electronic Materials published by Wiley-VCH GmbH. This is an open access article under the terms of the Creative Commons Attribution-NonCommercial License, which permits use, distribution and reproduction in any medium, provided the original work is properly cited and is not used for commercial purposes.

DOI: [10.1002/aelm.202001166](https://doi.org/10.1002/aelm.202001166)

transistors' operation voltage from tens of volts to just less than 3 V, due to their large capacitance (typically in the order of 1–10  $\mu\text{F cm}^{-2}$ ) and high ionic conductivity ( $>10^{-4}$  S  $\text{cm}^{-1}$  at room temperature (RT)).<sup>[26–30]</sup> Within this category of electrolytes, we have already proposed an innovative and versatile generation of reusable, recyclable, sticky, and highly conformable regenerated cellulose-based electrolytes.<sup>[31]</sup> Their formulation consists of dissolving microcrystalline cellulose (MCC) and carboxymethyl cellulose (CMC) at low temperature ( $<-8$  °C) using an aqueous lithium hydroxide (LiOH)/urea solvent system, followed by regeneration of cellulose with acetic acid. This approach is very simple, rapid, safer, and more environmental friendly in comparison with other organic solvents dissolving cellulose by heating method.<sup>[32]</sup> The developed lithium-based cellulose ionic conductive hydrogels (Li-CICHs) were successfully implemented as high-capacitance gate dielectrics in flexible, low-voltage ( $<2$  V) amorphous indium gallium zinc oxide (IGZO) electrolyte-gated transistors (EGTs) on multilayer-coated paper using an innovative, smart, and user-friendly approach. Such approach consists of directly applying the electrolyte, as a sticker, onto devices, decreasing considerably the time and degree of complexity of manufacturing.

Yet some concerns can arise regarding the use of lithium due to the huge stress on the demand for this element and its limited abundance.<sup>[33–35]</sup> One foreseen alternative is sodium, due to its low cost (ratio of costs for carbonate Li:Na = 100:3),<sup>[34]</sup> nontoxicity, high abundance (the sixth most abundant element in the Earth's crust), and chemical similarity with lithium. Here, we report the development of self-healable, adhesive sodium-based CICHs (Na-CICHs), where NaOH is used as a more environmentally friendly and less expensive alternative than LiOH for cellulose dissolution. The unique combination of electrochemical performance, facile preparation, efficient healing ability (after formation of undesirable dendrites or physical damage of the CICHs) due to reversible hydrogen-bonding, and recyclability holds the promise for their application in sustainable low-power, flexible ion-controlled electronics (iontronics).<sup>[36]</sup>

Low-voltage flexible IGZO EGTs and integrated logic circuits onto paper-based substrates are demonstrated. Basic handwriting accessories, including a commercial silver-based ink rollerball pen and a pencil, are used for easy patterning of conductive/resistive paths “on-the-fly” by merely drawing them out on paper, without the need of sophisticated, time-consuming and expensive techniques.

## 2. Results and Discussion

### 2.1. Formulation and Characterization of the Self-Healable Cellulose Iontronic Stickers

As illustrated in Figure S1 in the Supporting Information, the formulation of the CICHs consists of the dissolution of mixtures of MCC and CMC in precooled aqueous alkali hydroxide solvent systems, such as LiOH/urea and/or NaOH/urea, followed by regeneration with acetic acid.<sup>[32]</sup> Since Na has some similar chemical properties when compared with Li, the inclusion complex (IC) model is also the mechanism accepted for

cellulose dissolution at low temperature.<sup>[32,37,38]</sup> The addition of acetic acid breaks the cellulose IC, thus exposing the hydroxyl groups of cellulose that in turn induces the self-aggregation of cellulose to form rapidly physical hydrogels.<sup>[39]</sup>

In order to get a reliable comparison on the influence both alkali hydroxides in the properties of the CICHs, the concentration of NaOH used for dissolution of cellulose was the same as the typically reported for LiOH (4.6 wt%) in urea (15 wt%)/water solvent system.<sup>[32]</sup> Several mixtures of LiOH and NaOH were also prepared (LiOH:NaOH = weight ratio of 3:1, 1:1, 1:3, and 1:19), maintaining the weight ratio of alkali hydroxide in urea/water solvent system constant. The hydrogels obtained from LiOH:NaOH mixture (LN-CICHs) were named as L3N1, L1N1, L1N3, and L1N19, respectively. The hydrogels prepared from this method were compared with those prepared using just LiOH (referred to as L100) or NaOH (referred to as N100) in the cellulose dissolution.

The transparency of the solutions can be related with the efficiency of the dissolution process of cellulose. MCC dissolution has shown to be less effective in the aqueous NaOH/urea solvent system in comparison with the use of LiOH, since the smaller ionic radius of lithium ions ( $\text{Li}^+$ ) and its high charge density promotes an easier diffusion into the cellulose chain. One freezing–thawing cycle was performed to optimize cellulose dissolution since the concentration of NaOH used is lower than the ideal for an efficient dissolution, which according to literature is between 6 and 10 wt% at temperatures between  $-15$  and  $4$  °C.<sup>[40]</sup>

The resulting viscous MCC:CMC solutions after regeneration with acetic acid were shear-casted on glass and dried at RT, yielding flexible, robust, and sticky regenerated cellulose-based membranes with high conformability, as they can be easily molded and folded (Figure 1a). As exemplified in Figure 1b, the CICHs can be cut in the desired size and shape, peeled-off from glass, and transferred using tweezers to a device, like a sticker.

Figure S2a in the Supporting Information confirms the regeneration of cellulose with acetic acid.<sup>[41,42]</sup> Beyond the typical bands assigned to cellulose, fourier-transform infrared spectroscopy (FTIR) spectra in Figure S2b in the Supporting Information reveals additional bands in the CICH membranes due to the contribution of urea hydrates and regenerated cellulose. These results also reveal that water retention is higher in L100 hydrogel rather than N100, as smaller lithium ion tend to capture more water molecules than heavier alkali metal ions that are weakly hydrated.<sup>[43,44]</sup>

The smoothest surface of the CICHs (surface dried in contact with glass) is the one in contact with the semiconductor when used in EGTs to minimize the creation of interfacial defects between the functional layers (see Figure S3 in the Supporting Information).

Figure 2a shows the frequency dependence of the specific capacitance ( $C$ ) and phase ( $\theta$ ) for the different CICHs when sandwiched between two stainless steel electrodes (Nyquist plots are presented in Figure S4a in the Supporting Information). At low frequency ( $f < 1$  kHz), the specific capacitance is between 6 and 13  $\mu\text{F cm}^{-2}$  due to the formation of electrical double layers (EDLs) at the electrodes/CICH interfaces. The phase angle levels around  $-80^\circ$  due to a slightly nonideal capacitive behavior. The large specific capacitance values obtained for

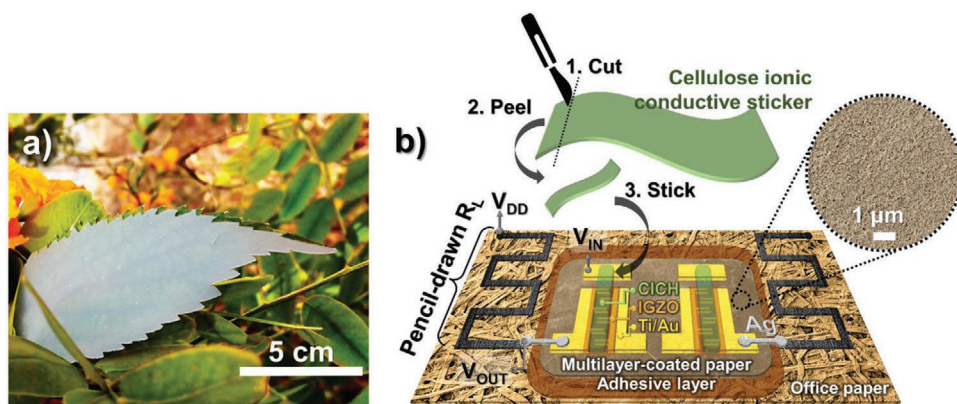


**Figure 1.** Schematic illustration of the manufacturing strategy for implementation of the CICHs onto flexible digital iontronic circuits. a) Photograph of the developed highly conformable and sticky Na-CICH, which was cut with the same shape of a leaf. b) Schematic illustration of two flexible planar CICH-gated IGZO EGTs fabricated on multilayer-coated paper integrated onto NOT gates with conductive/resistive tracks hand-drawn on office paper (inset: SEM image of the smooth and impermeable surface of the multilayer-coated paper substrate used for fabrication of the EGTs).  $R_L$ ,  $V_{DD}$ ,  $V_{OUT}$ , and  $V_{IN}$  stand for load resistance, supply voltage, output voltage, and input voltage, respectively.

Li-CICH, Na-CICH, and LN-CICHs are superior to traditional dielectrics and comparable with values typically reported for ion gels.<sup>[36,45]</sup> Such values persist up to the order of hundreds of Hz, decreasing significantly for higher frequencies, where ionic relaxation takes place.

Both electrical double layer capacitance ( $C_{DL}$ ) and ionic conductivity ( $\sigma_i$ ) were estimated from equivalent circuit model suggested by Dasgupta et al.,<sup>[46]</sup> calculated following the methodology presented in ref. [31] and plotted as a function of the

amount of NaOH used for cellulose dissolution (Figure 2b). All the results are listed in Table S1 in the Supporting Information.

The LN-CICHs exhibit high RT  $\sigma_i$  in the order of  $\approx 10^{-3}$  S  $\text{cm}^{-1}$  comparable to those of single small alkali metal ions ( $\text{Li}^+$ ). Nevertheless, there is a decrease in the  $\sigma_i$  for the CICHs obtained from high amounts of NaOH (L1N19 and N100 membranes), which can be related to a poorer water retention into these hydrogels, as verified by FTIR spectra in Figure S2b in the Supporting Information. The superior water retention ability of

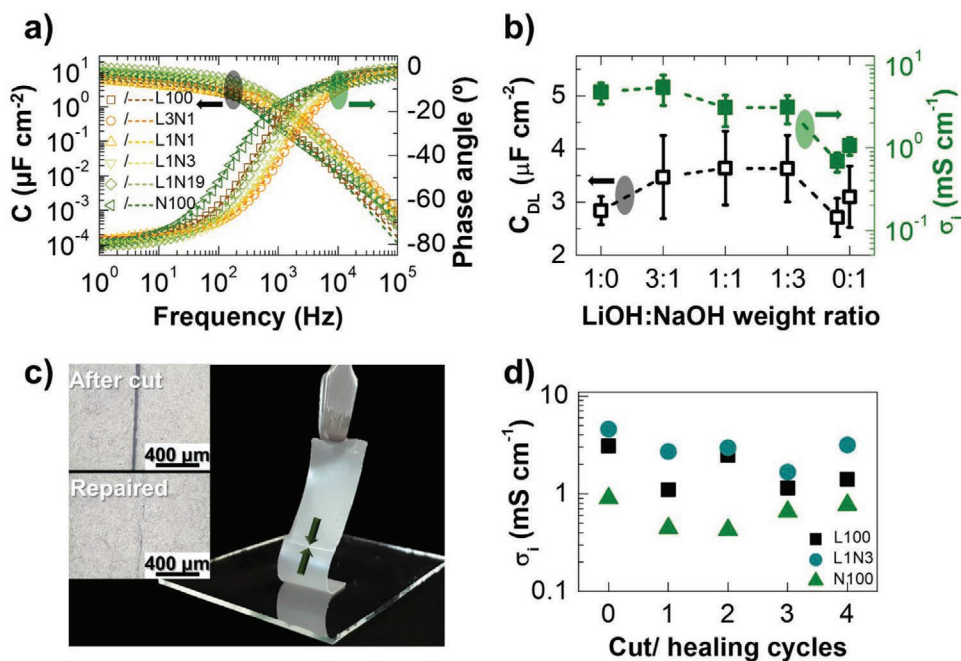


**Figure 2.** Electrochemical characterization of the developed CICHs. a) Capacitance and phase angle versus frequency plots of the original CICHs. The open symbols and the dashed lines denote the experimental data and the fitted data, respectively. b) Representation of  $C_{DL}$  and  $\sigma_i$  as a function of LiOH:NaOH contents used for cellulose dissolution. The data points show the average and corresponding error bars obtained from four samples. c) Photograph of the repaired N100 membrane after being cut into two pieces with a razor blade and then restored by gently pressing the pieces back into contact in the cutting region for 10 s (inset: optical microscope images of the N100 membrane in the cutting region after cut and repair). d) Ionic conductivity of the L100, L1N3, and N100 membranes after multiple breaking/healing cycles in the same position at RT.

lithium compared to sodium leads to additional free ionic species (protons and hydroxide anions) that aid in the process of ionic conduction.<sup>[31,44,47,48]</sup>

In this regard, some controversial results have been reported in literature and, therefore, there is not a consensual explanation.<sup>[49,50]</sup> Typically, smaller ions, such as Li<sup>+</sup>, result in higher conductivity than larger ions. However, the degree of hydration in aqueous medium is superior in alkali metal ions with smaller size, thus, increasing their effective size in water (hydrated ionic radius),<sup>[43]</sup> being less mobile. Although water molecules can lead to an increase in the amount of free ions, when in excess, it will reduce their mobility and hamper ion diffusion.<sup>[48]</sup> We must also consider the affinity of the hydrated ions with hydrophilic functional groups existing in the structuring polymers, such as the case of the hydroxyl and carboxymethyl, and the contribution of protons for the measured  $\sigma_i$ .

Despite such controversy, the lower values of  $\sigma_i$  obtained for the electrolytes that are highly enriched with sodium ions (Na<sup>+</sup>) can also be related to a less efficient dissolution of cellulose in aqueous alkali hydroxide/urea systems with higher contents of NaOH, which are also more prone to formation of dendrites composed of urea as confirmed by X-ray diffraction (XRD) (see Figure S5a,b in the Supporting Information). Figure S5c in the Supporting Information shows that these “tree-like” structures start forming in a relatively short time (less than 28 h) on the top surface (exposed to air during drying) of the membranes obtained from solutions with larger amounts of NaOH (L1N19 and N100 membranes), right after being cut and laminated for testing. Once the dendrites formation has started, the growth is spontaneous and continuous, leading to a gradual loss of transparency while the membranes become more brittle. Thus, there is a clear reduction of their conformability and adhesion to the substrate, leading to large interfacial resistances that negatively affect the electrochemical properties of the electrolytes.

The voltage window stability of the developed CICHs was evaluated by cyclic voltammetry (CV) (see Figure S4b in the Supporting Information), which has been found in the range from -2.5 to 2.5 V, that is suitable for the intended application as gate dielectric in transistors.

Considering the presence of hydrogen bonds in the developed CICHs (see Figure S2b in the Supporting Information), cut/healing tests were performed under ambient conditions to assess the healing capability of the CICHs. For these tests, the L100, L1N3, and N100 electrolytes were cut into two parts with a razor blade, and then the fragments were instantly merged into a single one by pressing them back together in the cutting region for 10 s (see Figure 2c and Video S1 in the Supporting Information). Figure 2d shows the ionic conductivity of the electrolytes after repeated cutting-off and contact-healing (see also Figure S6 in the Supporting Information). The results suggest that the two fragments, after being brought back into contact, can rapidly reestablish the network at the interface through the formation of physically crosslinked domains by reversible hydrogen bonding, mediated by either hydroxyl or amide groups.<sup>[10–16,48]</sup> As a result, the CICHs can restore their electrochemical properties by combining pressure with their self-healing characteristic, keeping the  $\sigma_i$  in the same range of values. By doing so, waste membranes can be recombined, shaped into the intended shape, and reused.

## 2.2. Electrical Performance of the Flexible CICH-Gated IGZO Transistors

Electrical characterization of the fabricated CICH-gated IGZO transistors on paper-based substrates was performed in air under ambient conditions, right after transfer and sticking of the electrolyte onto the devices. As shown in the inset of Figure 1b, the nanoporous top-coating layer of the multilayer-coated paper substrate was used to host the EGTs owing to its smoother and hydrophilic surface as well as good barrier properties.<sup>[51]</sup>

Figure 3 shows typical cyclic transfer (drain current  $I_{DS}$  vs gate voltage  $V_{GS}$ ), in saturation regime, and respective output ( $I_{DS}$  vs drain voltage  $V_{DS}$ ) curves of the flexible EGTs on paper. Important figures of merit, such as turn-on voltage ( $V_{ON}$ ), on/off current ratio ( $I_{ON/OFF}$ ), transconductance ( $g_m = \partial I_{DS} / \partial V_{GS}$ ) per channel width ( $g_m/W$ ), subthreshold gate voltage swing ( $S_S$ ), and saturation mobility ( $\mu_{sat}$ ), are summarized in Table S2 in the Supporting Information and plotted as a function of the amount of NaOH used for cellulose dissolution (see Figure S7 in the Supporting Information). The parameters  $S_S$  and  $\mu_{sat}$  were calculated according to Equations (S1) and (S2) in the Supporting Information, respectively. The values shown represent a statistical average of measurements performed for five devices, and respective errors. The electrical parameters were calculated in the forward sweep direction and in the saturation regime ( $V_{DS} = 1.2$  V).

The fabricated flexible CICH-gated EGTs are enhancement n-type transistors, which is confirmed by positive  $V_{ON}$  (0.04–0.18 V), and exhibit  $I_{ON/OFF}$  ratio larger than  $10^4$ , low  $S_S$  up to  $0.26$  V  $\text{dec}^{-1}$ , and the  $\mu_{sat}$  average values were calculated to be around  $3.4$  and  $6.9$   $\text{cm}^2$   $\text{V}^{-1}$   $\text{s}^{-1}$ . The devices operate at low  $V_{GS}$  (<2 V) showing a small hysteresis window with clockwise direction related to charge carrier trapping effects close the IGZO/CICH interface, indication that is not determined by ion relaxation in the electrolyte.

It is clear from the results that the nature of cations has influence on the electrical performance of the different CICH-gated transistors. The devices gated by L100 membrane achieve the highest performance reaching an  $I_{ON/OFF}$  of  $8.97 \times 10^4$  and a  $\mu_{sat}$  of  $5.3$   $\text{cm}^2$   $\text{V}^{-1}$   $\text{s}^{-1}$ , comparing with EGTs gated by N100 electrolyte that reach  $1.85 \times 10^4$  and  $3.4$   $\text{cm}^2$   $\text{V}^{-1}$   $\text{s}^{-1}$ , respectively. As aforementioned, the slight differences observed are directly related with the quick and unstable formation of urea dendrites in the latter electrolyte that negatively affects its mechanical properties and the adhesion to the semiconductor surface, as expressed also by the slight increase of  $S_S$  with the increase of NaOH. Nevertheless, EGTs gated by LN-CICHs have an electrical performance comparable with those gated by Li-CICH.

The output characteristics of the flexible EGTs demonstrate a linear behavior at low  $V_{DS}$  values together with a clear pinch-off and saturation for higher  $V_{DS}$  values, while the current levels in the output characteristics decrease for increasing levels of Na<sup>+</sup> in the CICH composition.

EGTs using the LN-CICHs formed from solutions with the two highest concentrations of NaOH (L1N3 and L1N19 membranes) were subjected to 250 successive  $V_{GS}$  cycles with a delay of 5 min between each scan, and their performance was compared with L100 membrane (see Figure S8 in the Supporting



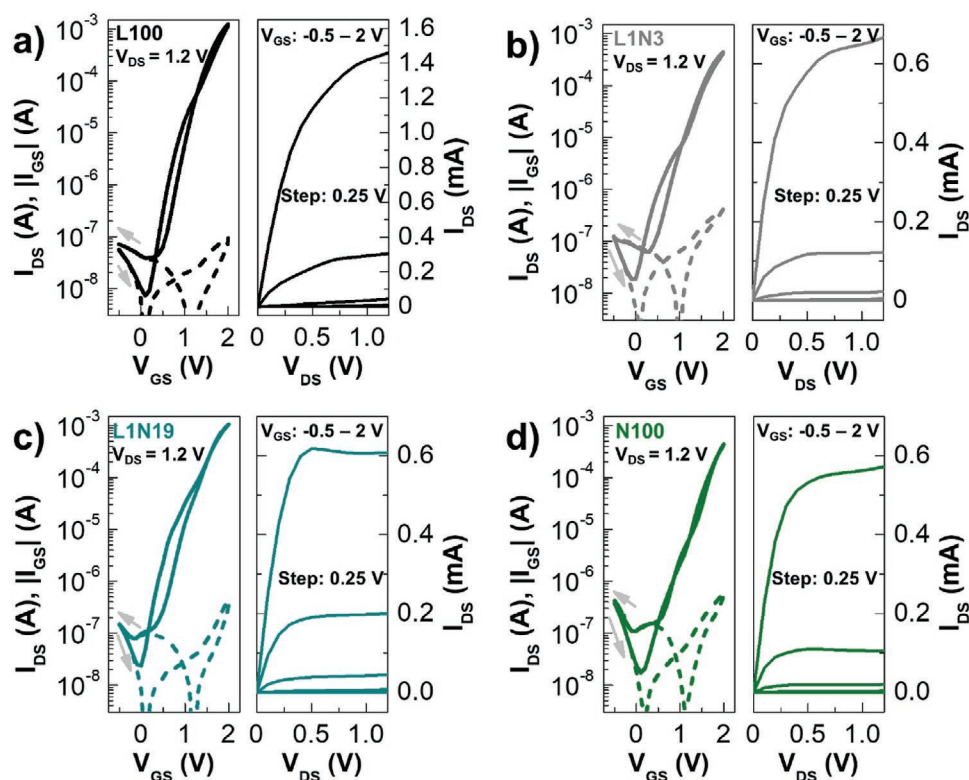


**Figure 3.** Electrical characteristics of the fabricated planar CICH-gated IGZO transistors on multilayer-coated paper. Cyclic transfer characteristic curves for saturation regime at  $V_{DS} = 1.2$  V ( $I_{DS}$ ,  $|I_{GS}|$  vs  $V_{GS}$ ) of IGZO EGTs gated by a) L100, b) L1N3, c) L1N19, or d) N100 membranes, and respective output curves ( $I_{DS}$  vs  $V_{DS}$ ) obtained for a  $V_{GS}$  step of 0.25 V starting at  $-0.5$  until 2 V. For the transfer curves, arrows represent the sweep direction, whereas continuous and dashed lines correspond to drain ( $I_{DS}$ ) and leakage ( $I_{GS}$ ) currents, respectively. All curves were acquired with a  $V_{GS}$  scan rate of 50 mV s<sup>-1</sup>.

Information). The devices gated by L100 or L1N3 membranes do not show significant signs of degradation. On the other hand, it is clear a degradation of the EGT's performance using the L1N19 membrane after around 150 cycles, as the dendrites start appearing.

Considering the hydrogel-nature of the CICHs, the environmental conditions affect the amount of water retained into their structure and, therefore, its swelling behavior. Thus, the role of temperature and relative humidity (RH) on the electrical performance of the EGTs was also undertaken (see Figures S10 and S11 in the Supporting Information). The L1N3 electrolyte was used for these measurements due to its superior environmental stability overtime in comparison with the CICHs with higher amounts of NaOH, as well as similar thermal behavior (see Figure S9b in the Supporting Information) and electrochemical properties to the L100 membrane.

The temperature range at which the devices were tested was limited to 100 °C, as the CICHs and paper substrate show some signs of degradation for higher temperatures (see Figure S9a in the Supporting Information). It is worth to mention that the layers deposited on paper are not expected to be significantly deformed with the swelling of the fibers, since it loses only a small amount of adsorbed water (4.2% of its weight) on the cellulose fibers at 100 °C.

There is a clear change of the electrical parameters with heating, demonstrating a steep degradation of the electrical

performance for temperatures higher than 50 °C due to the water release, resulting in the loss of ionic conductivity and adhesion to the semiconductor surface.<sup>[10]</sup> As temperature increases until 100 °C,  $I_{ON/OFF}$  is substantially affected decreasing to one order of magnitude as a result of the increase of  $I_{OFF}$  and considerable decrease of  $I_{ON}$ . During heating,  $V_{ON}$  shifts in direction to negative  $V_{GS}$  values due to thermal activation of the intrinsic conductivity of the semiconductor, which also explains the increase of  $I_{OFF}$  (see Table S3 in the Supporting Information).<sup>[52]</sup>

A very similar behavior was observed after testing a device overtime under vacuum conditions to study the influence of the RH (see Table S4 in the Supporting Information). In this case, it is remarkable the stability of the device as pressure drops inside the chamber down to  $4.2 \times 10^{-3}$  mbar, showing still some electrical modulation (inferior to one order of magnitude) at very low pressure levels ( $\approx 7.4 \times 10^{-4}$  mbar). The presence of hygroscopic alkali metal ionic species in the hydrogels aids in water retention even in environments with low RH.<sup>[53]</sup>

Also important to mention is the fast recovery of the electrical performance of the EGTs within a few minutes when exposed again to ambient conditions ( $24 \pm 2$  °C,  $43 \pm 4\%$  RH). In both cases, during cooling or after exposing the devices to atmospheric pressure conditions,  $I_{ON/OFF}$  reaches the same range of values obtained for pristine devices, despite both  $I_{OFF}$  and  $I_{ON}$  shift to higher values. This behavior demonstrates that this shift is determined by the IGZO rather than the electrolyte.

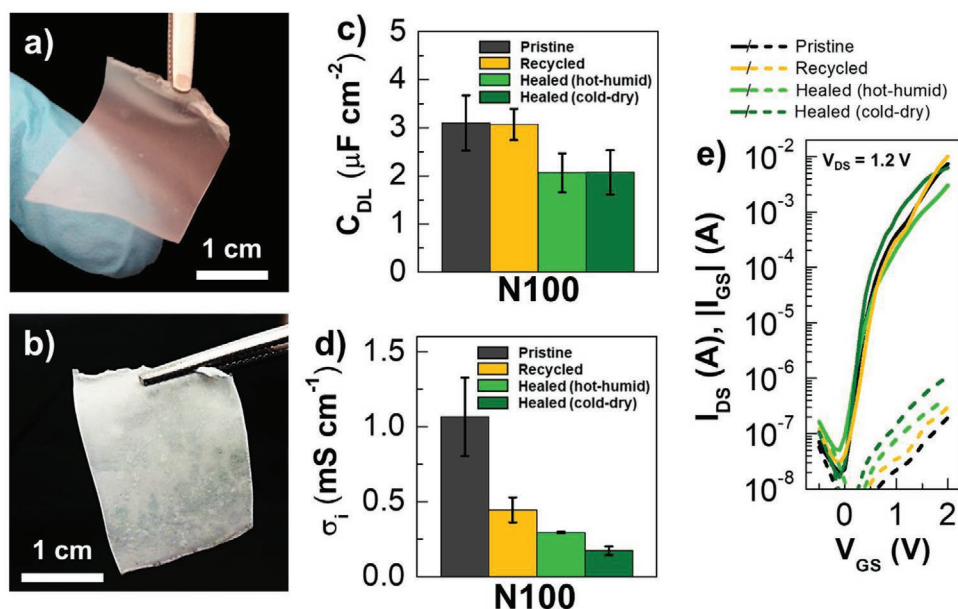


**Figure 4.** Self-healing ability and recyclability of the freestanding N100 iontronic hydrogel. Photographs of the freestanding N100 ionic hydrogel a) before and b) after formation of dendrites. Comparison of c)  $C_{DL}$  and d)  $\sigma_i$  for the different N100 membranes (pristine, recycled, healed - hot-humid environment, and healed - cold-dry environment). The data points show the average and corresponding errors bars obtained from four samples. e) Transfer characteristic curves of sputtered IGZO transistors on glass gated by pristine, recycled, or self-healed N100 ionic hydrogels recovered from exposure to hot-humid or cold-dry environment ( $V_{DS} = 1.2$  V,  $V_{GS}$  scan rate =  $50$  mV  $s^{-1}$ ).

These results also demonstrate that the electrolyte can spontaneously recover its performance overtime under ambient conditions without any external stimulus, due to the charged hydrophilic functional groups on cellulose chains that are able to attract the ions within the network, whereas large amounts of water are reversibly adsorbed in the framework.<sup>[10]</sup>

Another important point is that the reversible water retention of the electrolytes prepared from solutions with high levels of NaOH can delay or even reverse the formation of dendrites. The self-healing ability through a hydration process and recyclability was further explored in the N100 membrane, which is more prone to dendrite formation (Figure 4a,b; Video S1, Supporting Information).

The hydrogel was cut into two fragments and stored in a closed box with controlled environment ( $T = 24 \pm 2$  °C,  $33 \pm 2\%$ RH) until both were completely covered by dendrites ( $\approx 1$  day). One of the fragments was exposed for 2 h to water vapor, mimicking a “hot-humid” environment. The other fragment was kept inside a freezer at  $-25$  °C overnight, simulating a “cold-dry” environment. The membranes obtained from both experiments were then kept in a controlled environment at  $24 \pm 2$  °C and  $33 \pm 2\%$ RH for one day, and tested right after exposing them to ambient conditions ( $\approx 45$ – $50\%$ RH).

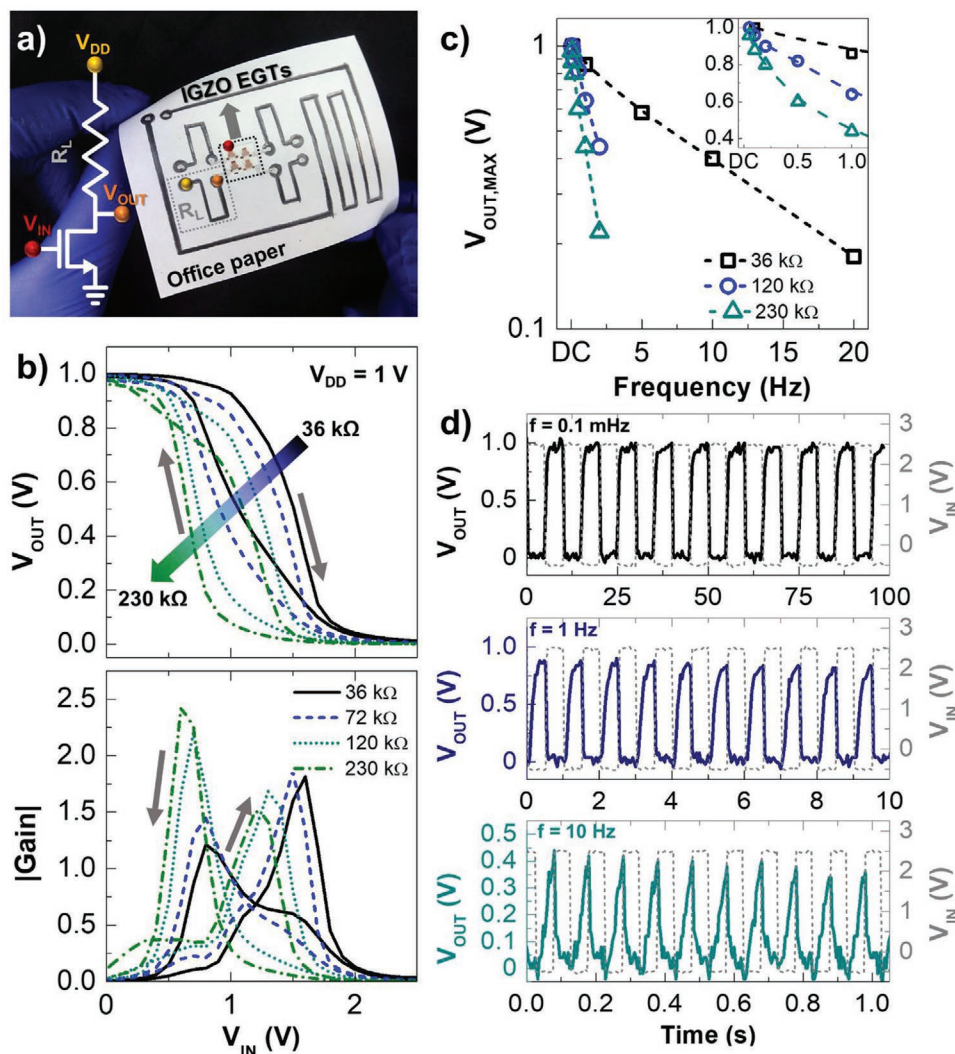
In both cases, the rehydration of the N100 membranes promotes the solubilization of urea dendrites in water, thus promoting their healing. Yet, the electrochemical performance of the healed hydrogel membranes is very distinct in comparison with the pristine membranes, as the performed hydration treatments influence the water content retained in the membrane that aid the healing process.

Figure 4c,d (see also Figure S12 and Table S5 in the Supporting Information) confirms that both approaches are

suitable to repair the N100 membranes after occurring the unwanted formation of dendrites at the cost of smaller  $\sigma_i$  with a difference of almost one order of magnitude. The membranes repaired in a “hot-humid” environment exhibit a better electrochemical performance ( $\sigma_i \approx 0.29$  mS  $\text{cm}^{-1}$ ), as the rehydration occurs faster when compared with those exposed to a “cold-dry” environment ( $\sigma_i \approx 0.17$  mS  $\text{cm}^{-1}$ ). In the latter case, the rehydration only starts when the membrane is stored inside the closed box in a relatively dry environment. This leads to a slower but not complete recovery of the membrane, as only a limited number of hydrophilic groups of cellulose are in an active state to promote self-healing.<sup>[48]</sup>

Although repair or reuse are far kinder strategies for a proper implementation of the circular economy concept, recycling is also a very attractive and sustainable strategy to address the negative impact of waste on the natural environment. The N100 hydrogels can be easily disassembled from IGZO transistors, and then efficiently recycled by soaking the membranes in water under stirring to obtain a homogeneous solution, and a new recycled membrane was prepared in the same way as the pristine. In a similar way as the healed membranes, a loss of electrochemical performance is observed in the recycled N100 membrane, where  $\sigma_i$  decreased nearly 58% (from  $1.07$  to  $0.45$  mS  $\text{cm}^{-1}$ ) (Figure 4c,d).

Considering the electrochemical performance displayed by the healed and the recycled N100 membranes, they can be successfully reused as gate dielectric in IGZO EGTs with comparable performance to devices gated by pristine counterparts (Figure 4e). The electrical parameters obtained for each device is displayed in Table S5 in the Supporting Information, and further comments are provided.



**Figure 5.** Electrical characterization of the flexible planar NOT gates on paper-based substrates. a) Photograph of the fabricated flexible planar NOT-gates with IGZO transistors gated by N100 membrane and pencil-drawn resistive tracks (inset: circuit schematic). Voltage transfer characteristics for different load resistances along a pencil-drawn graphitic line (arrows represent the sweep direction): b)  $V_{OUT}$  versus  $V_{IN}$ , and  $|gain|$  versus  $V_{IN}$ . c) Variation of maximum  $V_{OUT}$  ( $V_{OUT,MAX}$ ) with frequency for different resistances along a pencil-drawn graphitic line to an input square wave pulse from  $V_{IN} = -0.5$  to  $2.5$  V and  $V_{DD} = 1$  V after five cycles. d) Dynamic response of the flexible planar NOT gate with a pencil-drawn  $R_L$  of  $36$  k $\Omega$  to an input square wave pulse from  $V_{IN} = -0.5$  to  $2.5$  V and  $V_{DD} = 1$  V for  $0.1$ ,  $1$ , and  $10$  Hz.

### 2.3. Electrical Performance of the Flexible ClCH-Gated IGZO Circuits on Paper

Figure 5a shows four resistor-loaded inverters with planar sputtered IGZO EGTs on multilayer-coated paper gated by N100 membrane, and its respective circuit schematic. As schematized in Figure 1b, simple logic gate operations on paper substrates are demonstrated by adopting a hybrid manufacturing process that combines high-vacuum deposition techniques, to pattern the electrodes and the IGZO semiconductor of the transistors, with user-friendly room-temperature processes that allow the readily integration of the transistors into circuits. Regarding the latter set of processes, a transfer-lamination process is used to apply the electrolyte-sticker, while ubiquitous and portable handwriting accessories, such as a commercial silver-based ink

rollerball pen and a pencil, allow to easily draw the conductive/resistive tracks of the circuits.

Since the plastic coating of the multilayer-coated paper is not compatible with pencil-drawing, conventional office paper was used instead as its naturally rough surface allows the exfoliation of graphite particles, leading to the deposition of resistive tracks.<sup>[54]</sup> Thick electroconductive silver tracks are handwritten with a commercial pen to establish the connection between the drain electrode of the transistor fabricated on multilayer-coated paper and the pencil-drawn load resistance ( $R_L$ ) on office paper.

The circuit voltage transfer characteristics ( $V_{OUT}$  vs  $V_{IN}$  and  $|gain|$  vs  $V_{IN}$ ) are plotted in Figure 5b. A good signal inverting behavior is observed when switching  $V_{IN}$  from the “0” state ( $V_{IN} = 0$  V) to the “1” state ( $V_{IN} = 2.5$  V) for a drain voltage ( $V_{DD}$ ) of  $1$  V, meaning that if the applied input is low then the output



becomes high and close to  $V_{DD} - V_{th}$ , and vice versa. The  $V_{OUT}$  fully swept from near 1 V to almost 0 V with a relatively small output hysteresis. When increasing the  $R_L$  from 36 to 230 k $\Omega$ , the logic gate reaches a maximum  $|\text{gain}| (\partial V_{OUT}/\partial V_{IN})$  of 1.8 and 2.4, respectively. Owing to their low-voltage operation, thin-film batteries, supercapacitors, external radio frequency fields, or energy-harvesting systems can be used to power these logic gate circuits.<sup>[29,45,55]</sup>

Figure 5c demonstrates that the inverter can switch at rates in the 1–20 Hz range depending on the  $R_L$ . As shown in Figure 5d (see also Figure S12 in the Supporting Information), a better dynamic response is observed for lower values of  $R_L$  around of 36 k $\Omega$ . Higher operating frequencies, in kHz range, have already been reported in literature for EGTs and circuits.<sup>[56–60]</sup> The performance can be further improved by adopting transistors with submicrometric channel lengths, getting a better control of the overlap between source–drain electrodes with the thick electrolyte, and reducing the gate-channel distance, which can be with a top-gate geometry. Less capacitive probing or isolation of the output node with a buffer circuit can considerably improve the frequency of operation.

### 3. Conclusion

Highly conformable regenerated cellulose ionic hydrogels with high ionic conductivity ( $\approx 10^{-4}$ – $10^{-3}$  S cm $^{-1}$ ), reversible water retention and self-healing property (after formation of undesirable dendrites or physical damage) are successfully produced using a facile and “greener” preparation method based on NaOH/urea aqueous dissolution system of cellulose. These properties allied with their robustness and sticky surface enables their application as conformable electrolytic adhesives, making them suitable for integration in low-power flexible iontronics. This safe, user-friendly, and sustainable approach simplifies tedious and time-consuming device manufacturing processes, avoid the full replacement of the devices in case of damage and overtime usage, thus extending their lifetime and durability.

The CICHs were successfully applied as gate dielectric in flexible IGZO transistors on multilayer-coated paper exhibiting good performances ( $I_{ON/OFF} > 10^4$ ,  $\mu_{Sat} > 3.4$  cm $^2$  V $^{-1}$  s $^{-1}$ , and  $S_S < 0.26$  V dec $^{-1}$ ) under operating voltage below 2 V. Such devices can be integrated in basic low-voltage logic circuits, such as NOT gate, by sticking them on a sheet of paper, where conductive and resistive tracks are drawn with ubiquitous hand-writing accessories. By doing so, it is possible to fabricate low-cost, portable, disposable/recyclable smart iontronics capable of contributing for sustainable IoT.

### 4. Experimental Section

*Preparation of Self-Healable Cellulose Iontronic Stickers:* Following the procedure reported in the previous work,<sup>[31]</sup> different strategies for the dissolution of cellulose were employed. Cellulose dissolution medium was prepared by mixing 4.6 wt% LiOH (0.46 g, Sigma-Aldrich,  $\geq 98\%$ ) or NaOH (Labkem,  $\geq 98\%$ ), and 15 wt% urea (1.5 g, Carl Roth,  $\geq 99.5\%$ ) in 80.4 wt% deionized water (8.04 g, Millipore). Different

alkali hydroxide mixtures of LiOH and NaOH (LiOH:NaOH = weight ratio of 3:1, 1:1, 1:3, and 1:19) were also prepared, while keeping the weight ratio of 4.6 wt% alkali hydroxides mixture, 15 wt% urea, and 80.4 wt% of water (0.46 g of LiOH:NaOH, 1.5 g of urea, and 8.04 g of water in 10 g of solution). The solvent mixtures were precooled in a freezer at  $-25$  °C, until they became a frozen solid. The frozen solutions were then allowed to thaw at ambient conditions and 4 wt% of MCC (0.4 g in 10 g of solution, Sigma-Aldrich, powder: 20  $\mu$ m) was immediately added into the solvent system (9.6 g in 10 g of solution) under vigorous stirring at  $-8$  °C until its complete dissolution ( $\approx 30$  min). A freezing–thawing cycle was performed to improve cellulose dissolution.

Mixtures of MCC and CMC (Sigma-Aldrich,  $M_w \approx 250\,000$ ) with a weight ratio of 1:1 were prepared by adding CMC (0.4 g) to the previous cellulose solutions (10 g). The mixtures were stirred at RT conditions until CMC dissolution and then at  $-8$  °C to ensure MCC dissolution. The transparent solutions were kept overnight in a freezer at  $-25$  °C. The last step consisted of neutralization of the solutions and simultaneous regeneration of cellulose with acetic acid ( $\approx 1$  mL, Sigma-Aldrich,  $\geq 99$ ). This process was performed in an icy bath by slowly adding acetic acid drop-by-drop to the cellulose solution under stirring to avoid overheating. The resulting solutions were shear-casted on a glass plate. The  $\approx 1$  mm thick electrolyte films were dried in a closed box with controlled environment ( $T = 24 \pm 2$  °C,  $33 \pm 2\%$ RH) for 3 days and stored in air. The thickness of the resulting membranes was estimated from the average of five measurements made using a Mitutoyo digital micrometer.

*Characterization of Self-Healable Cellulose Iontronic Stickers:* Scanning electron microscopy (SEM) images of the different CICHs were acquired with a Carl Zeiss Auriga crossbeam (SEM-FIB) workstation instrument equipped with an Oxford energy dispersive X-ray spectrometer. The SEM images were acquired in the in-lens mode with an acceleration voltage of 2 kV and aperture size of 30  $\mu$ m. The cellulosic membranes were attached on aluminum stubs using a double-sided carbon tape and coated with a thin iridium layer ( $< 20$  nm) using a Q300T D Quorum sputter coater.

The structural analysis of the L100 and N100 electrolytes was done via XRD (PANalytical, model X'Pert Pro) using a PANalytical X'Pert Pro, with Bragg–Brentano geometry and Cu  $K\alpha$  line radiation ( $\lambda = 1.5406$  Å).

FTIR spectra acquisition was performed at RT, using an attenuated total reflectance sampling accessory (Smart iTR) equipped with a single-bounce diamond crystal on a Thermo Nicolet 6700 spectrometer. The spectra were acquired between 4000 and 525 cm $^{-1}$  with a 4 cm $^{-1}$ .

Thermogravimetric analysis measurements were performed with a simultaneous thermal analyzer (TGA-DSC - STA449 F3 Jupiter). Approximately 3 mg of each sample was loaded into an aluminum pan and heated from 25 to 550 °C with a heating rate of 5 °C min $^{-1}$ . All the measurements were carried out under air atmosphere.

Electrochemical characterization of the ionic hydrogels was carried out at RT ( $23 \pm 2$  °C,  $\approx 50\%$ RH) in a typical capacitor structure by depositing the electrolyte between two stainless steel discs with an active area of 1 cm $^2$ , using a Gamry Instruments Reference 600 potentiostat. Electrochemical impedance spectroscopy measurements were performed with 10 mV AC voltage in a frequency range of 1 to 10 $^5$  Hz. CV measurements were performed in a potential range between  $-3$  and 3 V at a fixed scan rate of 50 mV s $^{-1}$  and a collection of five successive cycles were acquired before analysis.

*Electrolyte-Gated Transistors and Integrated Logic Circuits Fabrication and Characterization:* A planar configuration was adopted based on titanium/gold (Ti/Au) bottom electrodes (source, drain, and gate) deposited on glass (Marienfeld) or multilayer-coated paper (Felix Schoeller type 3) in an interdigital architecture, followed by sputtering process of amorphous IGZO, working as the active oxide semiconductor, and the CICHs as the gate dielectric. The semiconductor channel and the electrodes were patterned by shadow masks with a channel width ( $W$ ) of 6800  $\mu$ m and length ( $L$ ) of 40  $\mu$ m ( $W/L = 170$ ). Gate-to-semiconductor gap was 50  $\mu$ m. A detailed description of the fabrication process of the developed flexible EGTs was given in the previous work.<sup>[31]</sup>



For circuits demonstration, ClCH-gated EGTs on multilayer-coated paper were glued with double-sided tape to a sheet of office paper (300%, Portucel Soporcel, Setúbal, Portugal). A resistor-load inverter was fabricated by exploiting pen-on-paper and pencil-on-paper approaches. Thick conductive tracks were drawn with a silver conductive ink rollerball pen (CircuitScribe) to establish the electrical connections between the drain electrode and the load resistance. Graphitic line tracks were hand-drawn with a HB-2 pencil (Black'Peps, Maped) to define the load resistances.

The EGTs and circuits were electrically analyzed in the dark in air at RT ( $24 \pm 2$  °C,  $43 \pm 4\%$ RH) using a microprobe station (Cascade Microtech M150) connected to a semiconductor parameter analyzer (Agilent 4155C) controlled by the software Metrics ICS. In situ temperature measurements were also performed using these equipments. The electrical characterization under vacuum was done in a Keithley 4200-SCS semiconductor parameter analyzer connected to a JANIS ST-500 microprobe station. For dynamic characterization, a microprobe station (Cascade Microtech MPS150) connected to a semiconductor parameter analyzer (Keysight B1500A) controlled by the software Keysight EasyEXPERT was used for biasing the circuit. A waveform generator was connected for input signal (Keysight 33500B Series) and the output signal was measured with an oscilloscope (ISO-TECH IDS 8062) with a high impedance probe (10 M $\Omega$ ). The oscilloscope cable and each probe of the microprobe station had a parasitic capacitance of 15 and 160 pF, respectively

## Supporting Information

Supporting Information is available from the Wiley Online Library or from the author.

## Acknowledgements

The authors acknowledge the support from FCT - Portuguese Foundation for Science and Technology through the Ph.D. scholarships SFRH/BD/126409/2016 (I.C.) and SFRH/BD/122286/2016 (J.M.). The authors would like to acknowledge the European Commission under project NewFun (ERC-StG-2014, GA 640598) and project SYNERGY (H2020-WIDESPREAD-2020-5, CSA, proposal n° 952169). This work was also supported by the FEDER funds through the COMPETE 2020 Program and the National Funds through the FCT - Portuguese Foundation for Science and Technology under the Project No. POCI-01-0145-FEDER-007688, reference UID/CTM/50025, project CHHC, reference PTDC/NAN-MAT/32558/2017. The authors would also like to thank their colleagues Daniela Gomes and Ana Pimentel from CENIMAT/i3N for the SEM and DSC-TGA measurements, respectively.

## Conflict of Interest

The authors declare no conflict of interest.

## Keywords

cellulose, electrolyte-gated transistors, electrolytes, logic gates, paper electronics, recyclability, self-healing

Received: November 30, 2020  
Published online: January 25, 2021

[1] M. Irimia-Vladu, *Chem. Soc. Rev.* **2014**, *43*, 588.

[2] A. S. Adila, A. Husam, G. Husi, in *2018 2nd International Symposium on Small-scale Intelligent Manufacturing Systems (SIMS)*; *IEEE* **2018**, pp. 1–5.

- [3] A. T. Vicente, A. Araújo, M. J. Mendes, D. Nunes, M. J. Oliveira, O. Sanchez-Sobrado, M. P. Ferreira, H. Águas, E. Fortunato, R. Martins, *J. Mater. Chem. C* **2018**, *6*, 3143.
- [4] R. Martins, D. Gaspar, M. J. Mendes, L. Pereira, J. Martins, P. Bahubalindruni, P. Barquinha, E. Fortunato, *Appl. Mater. Today* **2018**, *12*, 402.
- [5] M. Irimia-Vladu, N. S. Sariciftci, S. Bauer, *J. Mater. Chem.* **2011**, *21*, 1350.
- [6] D. Zhao, J. Huang, Y. Zhong, K. Li, L. Zhang, J. Cai, *Adv. Funct. Mater.* **2016**, *26*, 6279.
- [7] Z. Shi, G. O. Phillips, G. Yang, *Nanoscale* **2013**, *5*, 3194.
- [8] X. Shen, J. L. Shamshina, P. Berton, G. Gurau, R. D. Rogers, *Green Chem.* **2016**, *18*, 53.
- [9] L.-H. Fu, C. Qi, M.-G. Ma, P. Wan, *J. Mater. Chem. B* **2019**, *7*, 1541.
- [10] Z. Wang, H. Li, Z. Tang, Z. Liu, Z. Ruan, L. Ma, Q. Yang, D. Wang, C. Zhi, *Adv. Funct. Mater.* **2018**, *28*, 1804560.
- [11] J. Kang, J. B. H. Tok, Z. Bao, *Nat. Electron.* **2019**, *2*, 144.
- [12] S. Talebian, M. Mehrali, N. Taebnia, C. P. Pennisi, F. B. Kadumudi, J. Foroughi, M. Hasany, M. Nikkhal, M. Akbari, G. Orive, A. Dolatshahi-Pirouz, *Adv. Sci.* **2019**, *6*, 1801664.
- [13] D. L. Taylor, M. in het Panhuis, *Adv. Mater.* **2016**, *28*, 9060.
- [14] R. Tamate, M. Watanabe, *Sci. Technol. Adv. Mater.* **2020**, *21*, 388.
- [15] Z. Deng, H. Wang, P. X. Ma, B. Guo, *Nanoscale* **2020**, *12*, 1224.
- [16] Z. Wei, J. H. Yang, J. Zhou, F. Xu, M. Zrinyi, P. H. Dussault, Y. Osada, Y. M. Chen, *Chem. Soc. Rev.* **2014**, *43*, 8114.
- [17] S. H. Shin, W. Lee, S. M. Kim, M. Lee, J. M. Koo, S. Y. Hwang, D. X. Oh, J. Park, *Chem. Eng. J.* **2019**, *371*, 452.
- [18] H. Jia, X. Tao, Y. Wang, *Adv. Electron. Mater.* **2016**, *2*, 1600136.
- [19] K. Parida, V. Kumar, W. Jiangxin, V. Bhavanasi, R. Bendi, P. S. Lee, *Adv. Mater.* **2017**, *29*, 1702181.
- [20] I. Jeon, J. Cui, W. R. K. Illeperuma, J. Aizenberg, J. J. Vlassak, *Adv. Mater.* **2016**, *28*, 4678.
- [21] J. Ko, Y. J. Kim, Y. S. Kim, *ACS Appl. Mater. Interfaces* **2016**, *8*, 23854.
- [22] M. Khatib, T. Huynh, Y. Deng, Y. D. Horev, W. Saliba, W. Wu, H. Haick, *Small* **2018**, *15*, 1803939.
- [23] Y. J. Liu, W. T. Cao, M. G. Ma, P. Wan, *ACS Appl. Mater. Interfaces* **2017**, *9*, 25559.
- [24] Y. Cao, Y. J. Tan, S. Li, W. W. Lee, H. Guo, Y. Cai, C. Wang, B. C. K. Tee, *Nat. Electron.* **2019**, *2*, 75.
- [25] S. Bubel, M. S. Menyo, T. E. Mates, J. H. Waite, M. L. Chabiny, *Adv. Mater.* **2015**, *27*, 3331.
- [26] K. Hong, S. H. Kim, K. H. Lee, C. D. Frisbie, *Adv. Mater.* **2013**, *25*, 3413.
- [27] S. Thiemann, S. J. Sachnov, F. Pettersson, R. Bollström, R. Österbacka, P. Wasserscheid, J. Zaumseil, *Adv. Funct. Mater.* **2014**, *24*, 625.
- [28] J. Lee, L. G. Kaake, J. H. Cho, X.-Y. Zhu, T. P. Lodge, C. D. Frisbie, *J. Phys. Chem. C* **2009**, *113*, 8972.
- [29] Y. Xia, W. Zhang, M. Ha, J. H. Cho, M. J. Renn, C. H. Kim, C. D. Frisbie, *Adv. Funct. Mater.* **2010**, *20*, 587.
- [30] J. H. Cho, J. Lee, Y. Xia, B. Kim, Y. He, M. J. Renn, T. P. Lodge, C. D. Frisbie, *Nat. Mater.* **2008**, *7*, 900.
- [31] I. Cunha, R. Barras, P. Grey, D. Gaspar, E. Fortunato, R. Martins, L. Pereira, *Adv. Funct. Mater.* **2017**, *27*, 1606755.
- [32] X. Luo, L. Zhang, *Food Res. Int.* **2013**, *52*, 387.
- [33] A. Yaksic, J. E. Tilton, *Resour. Policy* **2009**, *34*, 185.
- [34] K. Vignarooban, R. Kushagra, A. Elango, P. Badami, B.-E. Mellander, X. Xu, T. G. Tucker, C. Nam, A. M. Kannan, *Int. J. Hydrogen Energy* **2016**, *41*, 2829.
- [35] G. G. Eshetu, G. A. Elia, M. Armand, M. Forsyth, S. Komaba, T. Rojo, S. Passerini, *Adv. Energy Mater.* **2020**, *10*, 2000093.
- [36] S. Z. Bisri, S. Shimizu, M. Nakano, Y. Iwasawa, *Adv. Mater.* **2017**, *29*, 1607054.
- [37] J. Cai, L. Zhang, S. Liu, Y. Liu, X. Xu, X. Chen, B. Chu, X. Guo, J. Xu, H. Cheng, C. C. Han, S. Kuga, *Macromolecules* **2008**, *41*, 9345.

- [38] J. Cai, L. Zhang, C. Chang, G. Cheng, X. Chen, B. Chu, *ChemPhysChem* **2007**, *8*, 1572.
- [39] M. He, Y. Zhao, J. Duan, Z. Wang, Y. Chen, L. Zhang, *ACS Appl. Mater. Interfaces* **2014**, *6*, 1872.
- [40] S. Zhang, F. Li, J. Yu, Y. Hsieh, *Carbohydr. Polym.* **2010**, *81*, 668.
- [41] J. Cai, L. Zhang, *Macromol. Biosci.* **2005**, *5*, 539.
- [42] S. Y. Oh, I. Y. Dong, Y. Shin, C. K. Hwan, Y. K. Hak, S. C. Yong, H. P. Won, H. Y. Ji, *Carbohydr. Res.* **2005**, *340*, 2376.
- [43] J. Mähler, I. Persson, *Inorg. Chem.* **2012**, *51*, 425.
- [44] P. Grey, S. N. Fernandes, D. Gaspar, J. Deuermeier, R. Martins, E. Fortunato, M. H. Godinho, L. Pereira, *ACS Appl. Electron. Mater.* **2020**, *2*, 426.
- [45] S. H. Kim, K. Hong, W. Xie, K. H. Lee, S. Zhang, T. P. Lodge, C. D. Frisbie, *Adv. Mater.* **2013**, *25*, 1822.
- [46] S. Dasgupta, G. Stoesser, N. Schweikert, R. Hahn, S. Dehm, R. Kruk, H. Hahn, *Adv. Funct. Mater.* **2012**, *22*, 4909.
- [47] L. Pereira, D. Gaspar, D. Guerin, A. Delattre, E. Fortunato, R. Martins, *Nanotechnology* **2014**, *25*, 094007.
- [48] D. Zhao, Y. Zhu, W. Cheng, G. Xu, Q. Wang, S. Liu, J. Li, C. Chen, H. Yu, L. Hu, *Matter* **2020**, *2*, 390.
- [49] C. Zhong, Y. Deng, W. Hu, J. Qiao, L. Zhang, J. Zhang, *Chem. Soc. Rev.* **2015**, *44*, 7484.
- [50] C. Zhong, Y. Deng, W. Hu, D. Sun, X. Han, J. Qiao, J. Zhang, *Electrolytes for Electrochemical Supercapacitors*, CRC Press, Boca Raton, FL, USA **2016**, pp. 31–254.
- [51] R. Barras, I. Cunha, D. Gaspar, E. Fortunato, R. Martins, L. Pereira, *Flexible Printed Electron.* **2017**, *2*, 014006.
- [52] J. Martins, P. Bahubalindrani, A. Rovisco, A. Kiazadeh, R. Martins, E. Fortunato, P. Barquinha, *Materials* **2017**, *10*, 680.
- [53] Y. Cao, T. G. Morrissey, E. Acome, S. I. Allec, B. M. Wong, C. Keplinger, C. Wang, *Adv. Mater.* **2017**, *29*, 1605099.
- [54] N. Kurra, G. U. Kulkarni, *Lab Chip* **2013**, *13*, 2866.
- [55] D. J. Gundlach, *Nat. Mater.* **2007**, *6*, 173.
- [56] B. Nasr, D. Wang, R. Kruk, H. Rösner, H. Hahn, S. Dasgupta, *Adv. Funct. Mater.* **2013**, *23*, 1750.
- [57] G. Cadilha Marques, S. K. Garlapati, S. Dehm, S. Dasgupta, H. Hahn, M. Tahoori, J. Aghassi-Hagmann, *Appl. Phys. Lett.* **2017**, *111*, 102103.
- [58] K. Hong, Y. H. Kim, S. H. Kim, W. Xie, W. D. Xu, C. H. Kim, C. D. Frisbie, *Adv. Mater.* **2014**, *26*, 7032.
- [59] M. Ha, J.-W. T. Seo, P. L. Prabhumirashi, W. Zhang, M. L. Geier, M. J. Renn, C. H. Kim, M. C. Hersam, C. D. Frisbie, *Nano Lett.* **2013**, *13*, 954.
- [60] L. Herlogsson, X. Crispin, N. D. Robinson, M. Sandberg, O.-J. Hagel, G. Gustafsson, M. Berggren, *Adv. Mater.* **2007**, *19*, 97.